BNT

Measurement of the Gravitational Constant

Jens H. Gundlach and Stephen M. Merkowitz*
Department of Physics, Center for Experimental Nuclear Physics and Astrophysics, University of Washington, Seattle, Washington 98195
(December 31, 2002)

We measured Newton's gravitational constant G using a torsion balance installed on a continously rotating turntable operated in acceleration feedback. Our technique was designed to eliminate or reduce several sources of uncertainty experienced by previous torsion balance measurements: Our torsion fiber was not twisted appreciably making the measurement insensitive to the fiber properties. A thin flat plate was used as pendulum eliminating uncertainties due to the pendulum density distribution. Four attractor spheres were rotated continously on a second coaxial turntable to separate the signal from the stationary gravitational room background. The signal was modulated at a relatively high frequency reducing $1/f$-noise. We obtained $G = (6.674255 \pm 0.000092) \times 10^{-11}$ m^3 kg^{-1} s^{-2}. Using results from the LAGEOS satellites, the Earth's mass is $M_\oplus = (5.972209 \pm 0.000082) \times 10^{24}$ kg and the Sun's mass is computed to be $M_\odot = (1.988423 \pm 0.000027) \times 10^{30}$ kg.

PACS numbers: 06.20.Jr, 04.80.-y, 06.30.Gv, 97.10.Nf, 91.10

I. INTRODUCTION

Historically the gravitational constant G, also referred to as Newton's Constant or sometimes Cavendish's constant was the first fundamental constant of physics to be measured in the laboratory. It is, along with Planck's constant $\hbar$ and the speed of light c, considered to be one of the most fundamental and universal constants in nature. Unlike most other physical constants, and despite the long history of measurements, the value of G has become the least precisely known fundamental constant in physics. The difficulty in measuring G is mostly due to the intrinsic weakness of gravity compared to the other interactions and the non-shieldability of gravity.

Since the first laboratory measurement by Cavendish over 200 years ago, the reduction in uncertainty in G has been slow: only an improvement of about a factor of ten per century was achieved. To make matters worse, measurements in the 1990's [1–7] all had larger error-bars than the value of Luther and Towler [8] on which the 1986 accepted value [9] was based. In addition, some of these measurements presented values far outside the ± 128 ppm 1-σ-uncertainty of the 1986 accepted value, bringing the accuracy of G into question. One of these carefully carried out and well documented measurements [2] yielded a value that was 0.6% higher or 42 of that measurement's standard deviations away from the accepted value. No definitive source that explains this outlier has been confirmed to date. Recognizing this situation, the 1998 recommended value was set to be $G = (6.673 \pm 0.010) \times 10^{-11}$ m^3 kg^{-1} s^{-2} [10], corresponding to an uncertainty of ± 1500 ppm, which is 12 times larger than the uncertainty of the 1986 recommended value.

Newton's constant may be combined with the precisely determined geocentric gravitational constant, $GM_\oplus$, to directly yield the mass of the earth and similarly the mass of the Sun and that of the planets. Even though currently no explicit technical or theoretical application for a precise value of G exists, its value may in the future be important to fundamental theories attempting to unify gravity with the known standard model of physics. Our group uses G in the laboratory routinely to calibrate other torsion balance instruments.

Because of its exquisite sensitivity to small forces, Cavendish-type torsion balance instruments traditionally have led to the most precise determinations of G. However, three major limitations were common to the best of these measurements. (1) The absolute metrology to determine the exact mass distribution of the (usually small) pendulum was difficult. For example: out of a total uncertainty budget of 64 ppm in the highly respected 1982 measurement by Luther and Towler [8] 48 ppm were associated with the metrology of all the pendulum parts. Below we will describe a simple pendulum geometry that practically eliminates the need for precise pendulum metrology. It was astonishing that this simple pendulum geometry had never been used explicitly. (2) Another large uncertainty was due to statistical noise. The source of this noise is twofold: (a) A simple metallic torsion fiber that is heavily loaded produces noise that has $1/f$-character. (b) Masses nearby the instrument may be moving during the measurement (people and vehicle traffic, ground water etc.) cause noise due to their gravitational interaction with the pendulum. For example a person approaching a typical apparatus (example again for ref. [8]) to within about 5 m would cause a sig-

*Now at NASA- Goddard Space Flight Center, Code 661, Greenbelt, MD 20771

nal equivalent to ≈10 ppm. The character of this noise is typically $1/f$. Additional noise with $1/f$-character can arise due to seismic vibrations, thermal fluctuations, vacuum fluctuations etc. In our measurement we reduced the effect of these $1/f$ noise sources by rapidly modulating the signal of interest. (3) A third limitation of traditional torsion balance measurements was only recently pointed out by Kuroda [11]. Anelasticity in the torsion fiber biases the results of the most commonly used time of swing method. This bias was quantitatively demonstrated in several specific tests [7,12]. A correction of the bias based on models or additional measurements may itself introduce considerable error. We were able to avoid this bias entirely by not twisting the torsion fiber.

Our new method avoids or reduces above described limitations by design. It was first introduced in [13]. The results of our measurement of G were first published in Physical Review Letters [14], but are described in more detail here.

II. METHOD

At the heart of this novel method is a torsion balance placed on a well-controlled turntable. This turntable is located between a set of attractor spheres. The turntable is first rotated at a constant rate (for example ≈1rev/20 min). The pendulum experiences a sinusoidal torque due to the gravitational interaction with the stationary attractor masses. This torque leads to a small twice-per-revolution angular deflection of the pendulum. A feedback is then turned on that changes the rotation rate of the turntable so as to drive the torsion fiber twist to zero, Fig. 1.

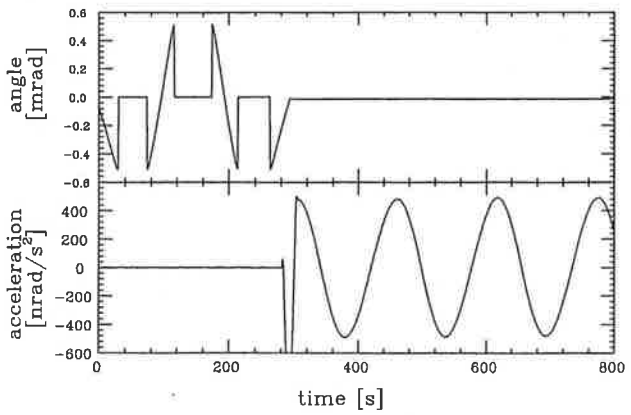

FIG. 1. Example of engaging the feedback to keep pendulum from twisting. At first the turntable was operated at a constant angular velocity. The pendulum experienced a twist which was a combination of its natural frequency (T ≈253 s) combined with the periodic gravitational torque (T ≈157 s). The twist angle exceeds the detector end-to-end range of about 1.0 mrad. At t=280 s the feedback was turned on. The pendulum experienced no noticeable twist and the signal of interest was contained in the turntable's angular acceleration.

The resulting angular acceleration of the turntable is now nearly equal to the gravitational angular acceleration of the pendulum. The angular acceleration rate is determined from the second time-derivative of the turntable angle readout. The torsion fiber does not experience any appreciable twist, and therefore this technique is insensitive to many torsion fiber properties including anelasticity, i.e. the Kuroda bias [11]. Additionally this method is inherently linear and the calibration of the angular acceleration is trivial once a full revolution is completed (360° =0°).

In 1969 Beams et al. [15] first used a rotating torsion balance with feedback. The Beams method produced a DC acceleration signal, unlike our method where the acceleration varied sinusoidally.

Another major advance realized by our apparatus may be illustrated by expanding the gravitational angular acceleration α of a torsion pendulum in spherical multipole moments [16]:

$$\alpha(\phi) = \sum_{l,m} \alpha_{lm} = -\frac{4\pi i G}{I} \sum_{l=2}^{\infty} \frac{1}{2l+1} \sum_{m=-l}^{+l} m \bar{q}_{lm} Q_{lm} e^{im\phi} , \tag{1}$$

where ϕ is the pendulum angle with respect to the source mass distribution, and I is the pendulum moment of inertia about the torsion fiber axis. The q_{lm} are the multipole moments of the pendulum:

$$q_{lm} = \int \rho(\vec{r}_p)\ Y_{lm}(\theta_p, \phi_p)\ r_p^l\ d^3 r_p\ . \tag{2}$$

Here $\rho(\vec{r}_p)$ is the density distribution of the pendulum. The Q_{lm} are the multipole fields of the external mass distribution:

$$Q_{lm} = \int \rho(\vec{r}_a)\ Y_{lm}(\theta_a, \phi_a)\ r_a^{-l+1}\ d^3 r_a\ , \tag{3}$$

with $\rho(\vec{r}_a)$ being the density distribution of the attractor. The $l = 1$ contributions in Eq. 1 vanish since a flexible torsion fiber allows the center of mass position of the pendulum to lie along the rotation axis (torsion fiber axis) hence $q_{11} = 0$. Because of the rapid convergence of the terms in Eq. 1 and the two-fold symmetric setup, by far the biggest contributions are the terms with $l = |m| = 2$ (terms with $m = \pm 2$ summed):

$$\alpha_{22}(\phi) = -\frac{16\pi}{5} G \frac{q_{22}}{I} Q_{22} \sin 2\phi \ . \qquad (4)$$

For an ideal, infinitely-thin two-dimensional vertical plate the quotient q_{22}/I, which contains all the pendulum properties, becomes a constant. The expression is independent of the pendulum mass distribution, $\rho(\vec{r}_p)$, i.e. mass, size, shape etc.:

$$\frac{q_{22}}{I} = \frac{\int \rho(\vec{r}_p) \ \ \frac{1}{4}\sqrt{\frac{15}{2\pi}} \sin^2\theta_p \ e^{2i\phi_p} \ \ r_p^2 \ d^3r_p}{\int \rho(\vec{r}_p) \ \sin^2\theta_p \ r_p^2 \ d^3r_p} \xrightarrow{2D} \sqrt{\frac{15}{32\pi}} \qquad (5)$$

and the dominant acceleration component is:

$$\alpha(\phi) \approx \alpha_{22}(\phi) = -\sqrt{\frac{24\pi}{5}} \ G \ Q_{22} \sin 2\phi \ . \qquad (6)$$

This flat pendulum geometry presents a significant advantage over previous torsion balance measurements, where the biggest contribution to the systematic uncertainty was due to the pendulum's mass distribution. Interestingly this cancelation had never before been used explicitly. For a thin rectangular plate with finite thickness t and width w a small and easily calculable modification must be applied to the ideal ratio:

$$\frac{q_{22}}{I} = \frac{w^2 - t^2}{w^2 + t^2} \sqrt{\frac{15}{32\pi}} \ . \qquad (7)$$

All other terms in Eq. 1 with $l > 2$ and $|m| = 2$ would also contribute to the signal of interest at $\sin(2\phi)$. These contributions were made to vanish by design or were very small and precisely calculable. Additionally the expansion in Eq. 1 converges rapidly as $(R_p/R_a)^{l-2}$, where R_p and R_a are the characteristic radii of the pendulum and of the attractor. All l = odd pendulum moments and attractor fields vanish due to the "up-down" symmetric design of the pendulum and the attractor masses. The $l = 4, |m| = 2$ contribution can also be eliminated by design: the q_{42} of a rectangular plate pendulum with height h vanishes by choosing $h^2 = \frac{3}{10}(w^2 + t^2)$, and additionally the Q_{42} of the attractor masses vanishes by using two spheres on each side of the pendulum with their centers spaced vertically by $z = \sqrt{2/3}\rho$, where ρ is the radial distance from the pendulum axis. With the above design the leading contribution to eqn. 1 becomes

$$\alpha_{22}(\phi) = -6 \left(\frac{6}{7}\right)^{\frac{5}{2}} \frac{GM}{\rho^3} \frac{w^2 - t^2}{w^2 + t^2} \sin 2\phi \qquad (8)$$

where M is the mass of one sphere. The lowest $l > 2, m = 2$ multipole order contribution in eqn. 1 that does not vanish by design is at $l = 6$. It is small and easily calculable:

$$\frac{\alpha_{62}}{\alpha_{22}} = \frac{99}{7683200} \frac{213(w^4 + t^4) + 626w^2t^2}{\rho^4} \ . \qquad (9)$$

Similarly, but even smaller, the α_{82} contribution is

$$\frac{\alpha_{82}}{\alpha_{22}} = \frac{351}{94119200} \frac{(139(w^4 + t^4) + 78w^2t^2)(w^2 + t^2)}{\rho^6} \ . \qquad (10)$$

Table I contains the numeric values of the α_{62} and α_{82} corrections for our setup.

The third major reduction in uncertainty was accomplished by placing the attractor spheres on a separate and coaxial turntable, that was rotated with angular velocity $\omega_a(t) = \omega_d + \omega_i(t)$, where $\omega_i(t)$ is the angular velocity of the torsion balance turntable. The *difference* angular velocity between the two turntables, $\omega_d = \dot{\phi}$, was held *constant* and was set by the operator. The gravitational constant was extracted by determining the amplitude of the angular acceleration of the pendulum turntable at $\sin(2\omega_d t)$. The rotation of the attractor masses allowed us to cleanly distinguish gravitational acceleration due to nearby stationary masses which occurred at $\sin(2\omega_i t)$. Furthermore, we were able to set the signal frequency at a relatively high frequency to suppress the $1/f$-noise characteristic of the torsion balance and of the gravitational noise background.

III. THE APPARATUS

A schematic view of the apparatus is shown in Fig. 2. A compact design was chosen, small enough so that the attractor masses could easily be handled by a person, but big enough to allow practical and precise metrology on the attractor masses. The intrinsic sensitivity requirement of this apparatus was much less stringent than in equivalence principle tests routinely performed with other rotating torsion balances at our laboratory. A 10 ppm uncertainty in G would be equivalent to an $\approx$8 nrad deflection angle resolution.

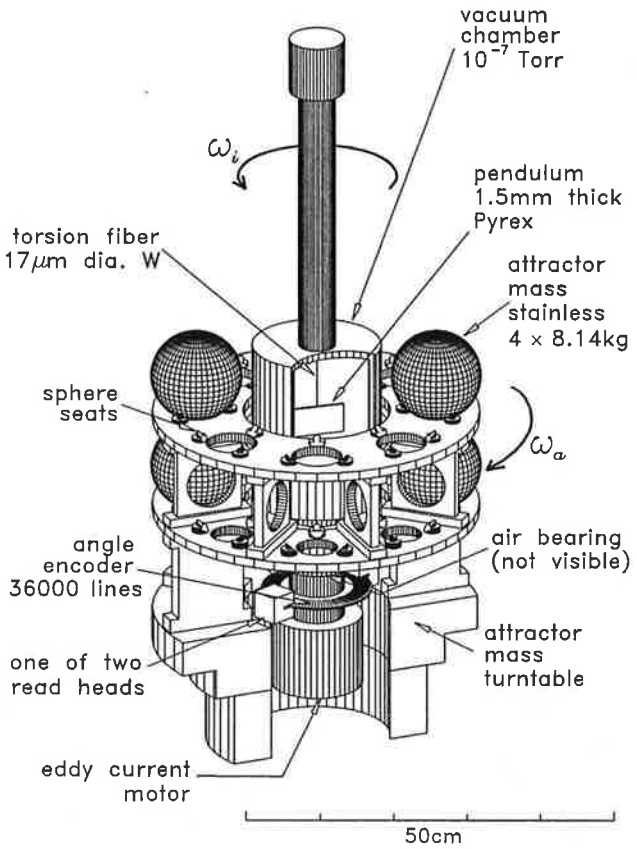

FIG. 2. Cut-away view of the apparatus.

A. torsion balance

The torsion pendulum body was located in cylindrically symmetric aluminum vacuum chamber with a 17.8 cm outer diameter and ≈6 mm wall thickness. It was enclosed by a 15 cm diameter, 1.5 mm thickness, μ-metal shield centered about the pendulum. The pendulum was suspended by a 41.5 cm long, 17 μm diameter uncoated tungsten torsion fiber with a restoring constant of about $\kappa = 0.035$ rad/erg. The top of the fiber was attached to a magnetic damper to reduce the pendulum swing mode. The swing damper consisted of a light-weight disk on a rod along the symmetry axis. The top of the rod was attached with a torsionally stiff, 2.5 cm long 76 μm diameter tungsten-"prehanger" fiber ($\kappa \approx 190$ rad/erg). The damper disk was centered between two permanent ring magnets. The B-field at the center of the disk was smaller than at the rim. The torsion fiber was mounted from the bottom of the rod. The natural rotational motion of the damper was not significantly damped and had an oscillation period of 0.62 s. Small copper crimps were used for all fiber attachments. Since the damper itself was cylindrically symmetric it experienced no gravitational torque, but it resisted the angular acceleration of the turntable twisting the prehanger and therefore the torsion fiber by about 5 nrad. This twist exerted a torque on the pendulum and lowered the measured acceleration of interest by 6.0 ppm. This effect, which had been omitted in our initial publication [14], resulted in a slight upward revision of our value of G. The effect is now included as a small correction factor in table I.

The prehanger fiber was attached to a vertical translation stage outside the vacuum. This stage in turn was mounted on a small motorized rotation stage.

The pendulum body was a 1.506 mm thick, 76 mm wide, and 41.6 mm tall Pyrex-glass plate. It was coated with a thin layer of chrome (≈ 50 nm) over which a thicker gold layer (≈ 150 nm) was evaporated. To attach the torsion fiber a small partially slotted aluminum cylinder was glued to the top of pendulum plate. This cylinder had a diameter of 3.2 mm and was 8.9 mm high. As this was an active part of the pendulum and departed from the simple plate geometry, this part, together with the tiny fiber crimp mounted in it, was carefully modeled and resulted in a small correction (table I). The total mass of the pendulum was about 11.9g. The pendulum was electrically grounded to the vacuum can through its torsion fiber. The pendulum rested in a light-weight Al-structure (catcher) when it was not supported by the torsion fiber. All parts near to the pendulum were Au-coated and electrically grounded.

The free oscillation period of the pendulum was ≈253 s. The uncompensated gravity signal would have caused a ≈0.8 mrad pendulum deflection.

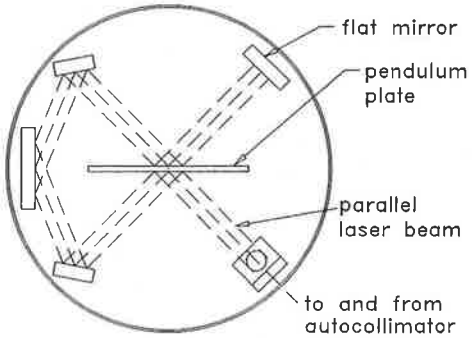

FIG. 3. Schematic view of the pendulum angle readout. The system is sensitive to a rotation perpendicular to the plane of the beams, i.e. rotations about the torsion fiber.

The small pendulum deflection angle was optically multiplied by 8 using two reflections of a light beam from the front and two reflections from the back of the pendulum plate. The angle multiplication optics, which is free of electronic noise, is illustrated in Fig. 3. This new optical angle amplification method is sensitive only to rotations about the torsion fiber but insensitive to all other rotations. The light beam originated from a PIN diode stabilized laser diode (model Sony SLD201,780 nm). It was passed through a circular divergence limiter (0.57° half angle) to form a 6 mm diameter parallel beam after passing through a 300 mm focal length lens. On the return path the reflected light passed through the same

lens but was diverted by a half-silvered beam splitter cube onto a 3 mm long linear position-sensitive detector (model UDT SL3-2). This detector was installed about 5 mm past the focal point to avoid non-linearity due to graininess of the detector material. The detector outputs were amplified and combined in low-noise electronics to produce Δ=(L-R) and Σ=(L+R), where L and R were the currents from the left and right side of the detector. Differential line drivers were used on all signal lines. The laser light was square wave modulated to allow lock-in detection. The pendulum twist angle was computed as $\Theta = k\Delta/\Sigma$ where k is a calibration constant. The laser beam power incident on the pendulum was estimated to be about <30 μW. The light beam hit the plate at the center. The small torque resulting from to the radiation pressure in combination with small misalignments could not change with the signal frequency and could therefore not produce a systematic error. The stationary mirror located at the far end of the beam path was tilted by about 3 mrad, so that the returning light passing straight through the beam splitter could not reach the laser diode and could not affect the laser power stabilization.

The vacuum chamber was initially pumped using a small turbo pump while it was baked to about 80 °C for several days. The bakeout, during which the torsion fiber supported the weight of the pendulum, drastically reduced the torsion fiber relaxation unwinding rate during the measurements. After the bakeout the turbo pump was removed and the vacuum was maintained with an 8 l/s ion pump. The ion pump was electrically isolated from the vacuum chamber. The residual pressure during data taking was about 2×10^{-5} Pa.

A single axis electronic precision level (Applied Geomechanics Inc. Model 755) was mounted radially on the vacuum can. The tilt was continually recorded and was used to level the turntable.

The apparatus was located close to the center of the round, mostly underground, former cyclotron cave of the Nuclear Physics Laboratory [17] at the University of Washington. The pendulum location was 3.5 m above the floor and >4 m from the nearest below ground wall and >30 m from the nearest vehicle traffic. The apparatus was installed on a massive platform consisting of the former yoke of the cyclotron. The platform was selected since it was measured to be seismically quiet, which is certainly due to its mass (200 tons of steel) resting on a solid concrete foundation. The gravitational Q_{22} moment at the location of the pendulum was measured using the apparatus itself. We chose to compensate the ambient Q_{22} using two 0.86 ton Cu blocks on opposite sides of the apparatus, about 0.75 m away. The remaining room background Q_{22} during the measurements was < 15 kg/m^3.

The partially underground room was temperature stabilized with a duty-cycle-free air conditioner operated in feedback to a temperature sensor near the apparatus. Temperature drifts and fluctuations were typically < 0.05 K/day. The instrument itself was in a passive thermal enclosure made of Styrofoam. The floor of the enclosure was not insulated but had a very long thermal time constant. The apparatus-temperature was measured in several places and recorded. Two calibrated thermistors were coupled to the aluminum attractor mass turntable. A slipring was used for the electrical signals. Offline the two attractor mass turntable temperature sensors were corrected for occasional glitches caused by the slipring imperfections and then averaged. A semiconductor temperature sensor (model AD590) was attached on the vacuum can near its center. A platinum air-thermometer was rotating with the vacuum chamber in the gap between the attractor mass turntable and the pendulum turntable. The room air temperature was measured using an AD590. The absolute temperature calibration was established with two calibrated thermistors and a calibrated mercury thermometer.

B. Turntables

The main component of the torsion balance turntable was a high precision air-bearing made by Professional Instrument Company of Minneapolis (model 4R, operated at 700 kPa). This bearing type was chosen for its nearly vanishing starting torque and small running friction. The apparatus platform was above the bearing, while directly below the bearing a 36,000 lines/revolution optical angle encoder was attached. This angle encoder made by the Heidenhein GmbH, Germany (model ERO725), was read with two readheads mounted oppositely. We used our own angle readout scheme described below. The torque to control the turntable was provided via a directly-mounted eddy-current motor consisting of a copper drag cup installed below the air bearing. A rotating field was produced around the cup with the stator of a high frequency 48-pole, 3-phase electric motor. The three phases were generated by the DSP feedback electronics (section III D).

All electrical connections to the torsion balance were through a 52-contact signal-quality slip ring assembly with the addition of a high voltage slipring for the ion pump. A small geared DC-motor supplied the torque to rotate the slipring. The slip ring rotation rate was locked to the inner turntable using a feedback loop with an optical interrupter as its sensor. The thin and soft electrical cables connecting the slipring assembly to the balance were attached with slack and adjusted to produce the minimal possible torque on the turntable. The turntable with the torsion balance apparatus on it was carefully balanced using small Pb-masses.

The attractor mass turntable had no direct mechanical connection to the torsion balance turntable. It was made from a large diameter, high-precision, dual angular contact degaussed steel bearing to which a 5 cm thick Al plate was bolted. An 18,000 line/rev optical angle encoder (Heidenhain, model ERA180.2003) with

one readhead was attached. A small geared DC motor was friction-coupled and was operated in a tight PID feedback to control the turntable at the desired rotation speed. The support structure for the attractor spheres was designed rigid but light-weight. The spheres were located each on three stainless steel seats with flat surfaces at 45° angles, tangential to the spheres. The seats themselves were embedded in machined recesses located in two shelves, which were made of cast-aluminum. Each shelve contained 8 symmetric positions to place spheres. The radius from the torsion fiber to the center of the spheres was ρ=16.51 cm and the vertical separation between the centers of the spheres was z =13.48 cm.

C. Attractor Masses

The attractor spheres were machined from the same selected bar of #316 stainless steel. The bar was ultrasonically tested for voids and density boundaries. No systematic density gradient along the length of the bar was found as determined from the volumes and masses of the manufactured spheres. The average diameter of the spheres was 124.89 mm. The diameter of each sphere was measured in 9 places which included the three diameters involved in the Q_{22} determination. A special sphere diameter measuring jig was constructed and calibrated with an Invar ball bar of nearly the same length as the sphere diameter. A small non-sphericity of the masses was discovered and included in the Q_{22} calculations. The RMS scatter of the diameter measurements on each sphere was on average 5 μm. The sphere mass was ≈8.140 kg [18]. A double substitution method was used as described by NIST Handbook 145 SOP 4. The balance was an equal-arm comparator, model Voland HCE25. The standard weights are traceable to NIST standards. The mass uncertainty (K=2 or 2σ) was 6 mg.

A pressure-dependent air-density correction had to be applied to the G-measurements. The air pressure was measured with an absolutely calibrated pressure sensor located a few hundred meters away in the atmospheric sciences building at the University of Washington and was corrected for a small elevation difference. Pressure data were recorded every minute and the average air density [19] during each data cut (about one hour) was computed. The absolute air-humidity was estimated and the uncertainty is reflected in the error budget.

The Q_{22} of the attractor mass configuration was ≈1900 kg/m^3 yielding a maximal angular acceleration on the pendulum of ≈4.9×10^{-7} rad/s^2.

D. Data Acquisition System and Experiment Controller

A digital signal processor (DSP) board (Spectrum 60 MHz, 32bit floating point processor, Texas Instruments TMS320C32) was used for primary data acquisition and control of the experiment. Sixteen 16-bit differential ADCs and eight 16-bit DACs were interfaced to the DSP. The DSP also controlled a stepper motor and several interlocks. The DSP code was written in C. The minimum execution time of DSP program loop was 250μs (4 KHz). The loop was triggered at precisely 2.5 KHz allowing for plenty of overhead time. This trigger rate was used for the overall timing. A 10 MHz signal from a temperature-controlled quartz oscillator (Model PTS 160) was divided down and the long term stability and calibration was established by comparing it to a once/second output from a GPS receiver. Over the duration of one month we found deviations of < 0.5 s. (additional checks were performed using NIST time via the Internet). At the end of each DSP loop cycle a counter was incremented that could be compared with the GPS clock to insure that no DSP cycles were ever lost or added. All the data were averaged by the DSP over exactly one second and uploaded to a PC pentium host computer for storage and online display.

The angle encoder produced one sine and cosine period for the passage of each of its 36000 stripes. These sine waves (typically 30 Hz) were digitized and the precise turntable angle was found by resolving the phase of each stripe using the DSP. A routine to remove a small higher harmonic content of the stripe signal could be invoked. The turntable angle readings from the two readheads of the pendulum turntable were averaged. A once per revolution marker served as an absolute angle reference and was used to verify that the angle readings remained accurate. The decoding of the attractor turntable angle readout was similar.

Two lock-in amplifier circuits were programmed into the DSP code for Δ and Σ. The lock-in frequencies were chosen to suppress 60 Hz line voltage. The pendulum angle was generated from the Δ and Σ. The signal was integrated with a 70 ms time constant. This signal became the input parameter to a proportional-differential-integral (PID) feedback loop that was also programmed into the DSP. The loop output controlled the position of the inner turntable such that the pendulum angle, i.e. the ratio Δ/Σ, remained at a constant value (which was set by the operator). The proportional and differential feedback function parameters were optimized by making the response to programmed angle steps fast and near-critically damped. The integral parameter was tuned to minimize the slow variations in θ (i.e. to maximize the feedback loop gain at the frequency of interest). A demonstration of the effectiveness of this feedback loop is shown in Fig. 1: In the feedback mode the pendulum had a "free" torsional period that approached ∞.

A similar PID feedback loop, which was also run with the DSP, controlled the outer attractor turntable. The input to that loop was $\phi_a + \omega_d t - \phi_i$, where ϕ_i and ϕ_a are the angles of the pendulum and attractor turntables and $\omega_d t$ was an internally created angle. ω_d set by the operator and held constant.

IV. PROCEDURES

A. Setup and Debugging

Commissioning of the apparatus was a gradual process in which we debugged and then optimized the performance of the new instrument. We took several month of explorative data during which we determined best running conditions (as for example turntable speeds, PID loop parameters, temperature control, etc.).

The inner turntable was leveled by requiring that the once per revolution signal of the level sensor was minimized. The turntable was releveled periodically between data runs. The vacuum can was aligned by minimizing the runout near the top of the vacuum can where the torsion fiber was attached. The torsion fiber was centered relative to the rotation axis of the rotation stage from which the fiber was mounted using a telescope. The two attractor-mass shelves were individually aligned radially to within 20 μm of the attractor turntable rotation axis. The attractor turntable was leveled with a precision spirit level and the horizontalness of the attractor shelves was verified with a dial indicator mounted on the inner turntable. Lateral centering of the attractor mass turntable axis relative to the pendulum turntable axis was established using dial indicators to better than <25 μm. A small 0.017° azimuthal misalignment between the upper and the lower attractor shelve was found and was included in the Q_{22} calculation. The vertical height of the attractor masses relative to the center of the pendulum was initially set using transfer marks. To verify and fine adjust the vertical centering of the pendulum to the attractor spheres, 8 spheres were placed on the turntable so that the Q_{32} was maximal. Using the vertical fiber positioner the resulting gravitational acceleration signal at $\sin 2\omega_d$ was zeroed by moving the pendulum to a position 0.29 mm lower than the position from the transfer marks.

Initially we had planned to conduct the G-measurement with 8 spheres at once [13] so that the signal would be bigger, but we found that the systematic error due to the more complicated metrology was larger than using only 4 spheres, while the statistical error increased only by $\sqrt{2}$.

Before taking the datasets for the actual G measurements we ran several preliminary data sets to identify large sources of systematic uncertainty so that we could make the necessary apparatus upgrades for the final measurement.

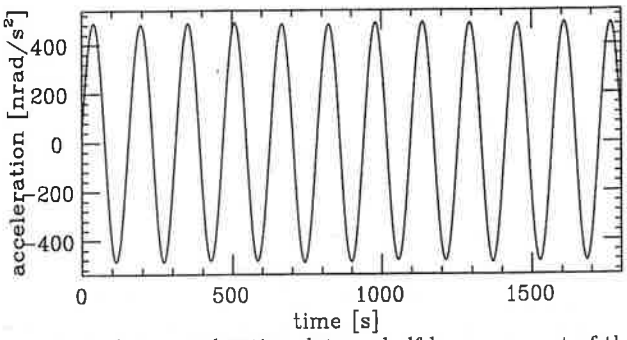

FIG. 4. Raw acceleration data: a half-hour segment of the twice numerically differentiated turntable angle. The signal frequency was constant and could be chosen by the operator.

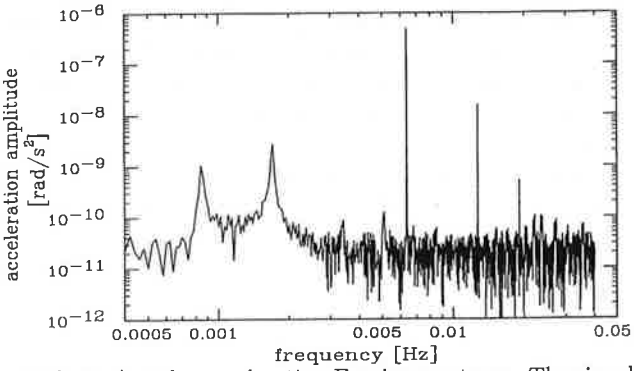

FIG. 5. Angular acceleration Fourier spectrum. The signal of interest($\approx$6.37 mHz) is more than four orders of magnitude above the random background. The room-fixed gravitational background ($\approx$1.7 mHz) is cleanly separated. The spectrum represents 10 hours of data.

B. Data Collection

We recorded six data runs, each approximately three days long, each with a different attractor mass configuration. A typical data segment is shown in Fig. 4 and a Fourier spectrum is shown in Fig. 5. Sets of two attractor mass configurations formed pairs that eliminated contributions from to the attractor turntable itself. The pairs consisted of attractor mass configurations with the spheres in two locations differing by 90° in azimuthal angle on the attractor turntable shelves. To average over density fluctuations and non-sphericity the spheres from the upper shelf were placed on the lower shelf and vice versa. Each sphere was also rotated about vertical by 180° so that a side of the sphere that faced the pendulum faced away from the pendulum. Three configuration pairs were taken with the sphere-internal x, y and z axis pointing towards the pendulum. Felt pen markings on the spheres were used to keep track of the orientations. We repeated the entire measurement cycle using four different spheres. The positions on the turntable that were not used with the first sphere set were used with the second sphere set.

The data with the first sphere set were taken between March 10th to April 1st, 2000. The second sphere set data were taken from April 3rd to April 18th, 2000. Since the noise performance during night time was significantly better, our measurement is dominated by data taken at night. Configuration changes were made during day time hours. We took data with each configuration until we had matching statistical uncertainties for each configuration.

For most of the data ω_i was set to $\approx$5.3 mrad/s and ω_d was set to exactly 20.01015 mrad/s so that the signal frequency occurred at $\approx$6.37 mHz and so that an integer number of data points per signal cycle were recorded. The frequency of the signal, the rotation frequency of the inner turntable and the rotation frequency of the outer turntable were chosen to be incommensurate, so that possible imperfections of the angle encoders were averaged out after the about 1500 signal cycles of a typical run. The signal frequency was selected to optimize the signal to noise ratio. We tested a wide variety of ω_i and ω_d and found the results for G independent of these angular velocities.

Improper equilibrium set point and fiber relaxation drift ($< 0.1\mu$rad/h if not run in feedback) changed the average rotation speed. The setpoint could easily be adjusted so that ω_i changed by less than 0.1 mrad/s over one day.

V. DATA ANALYSIS

The data were analyzed off-line using routines written in the program Matlab. The analysis procedures were designed to be autonomous, needing very little intervention from the user. The inner turntable position was numerically differentiated twice to yield angular acceleration. We chose data points 10 s apart to compute each derivative. Each data run was cut into sections (cuts). A variety of cut lengths were tested, but for the final analysis we used cuts 20π rad long in $\omega_d t$ signal phase (twenty sinusoidal cycles). Different starting phases for the cuts were also tested, each gave the same results within the statistical uncertainty.

The angular acceleration was fit for the sine and cosine amplitudes of the 2,4, and 8 ω_d signals, 1,2, and 4 ω_i signals, a drift term, and a DC offset. A number of fitting algorithms (regressions and fits) were tested all of which gave identical results within numerical errors. For the final analysis we used a linear least squares method.

Special criteria were set to automatically eliminate bad data sections. While the user would examine the raw data and fit results, it was unnecessary to manually remove bad data. The most simple criterion for rejection of a cut was the quality of the fit. If the root-mean-square of the fit residuals was larger than 5×10^{-9} rad/s^2 the cut was discarded. An example of a discarded cut is shown in Fig. 6. In this particular case we were able to identify the disturbance as caused by the implosion of the Kingdome sports arena.

FIG. 6. This data cut was automatically rejected. The disturbance is due to groundshaking from to the implosion of a large building about 7 km away. This cut was automatically removed by the analysis program.

Occasionally the pendulum would get a small "kick" that would show up as a small spike in the acceleration fit residuals. Most of these disturbances could be identified as a delta-function-like kick that would cause an instantaneous change in the pendulum's velocity (i.e. turntable velocity). These spikes would show up as a fixed width triangles in the numerically derived acceleration with their width entirely due to the time length used for the numerical derivatives. The nature of these kicks was clearly not gravitational. In similar experiments we found a correlation to a sudden rise in the ion pump current, i.e. vacuum pressure. An automatic search procedure identified the spikes in the acceleration fit-residuals and fitted their amplitudes. The spikes were then subtracted from the acceleration data and the data were fit again. If there were more than 4 spikes in a data-cut that exceeded a certain threshold, the entire cut was discarded. Fig. 7 shows the distribution of all identified spikes as a function of the signal phase. We found no correlation with the signal. We fitted the data without removing the spikes and found the results consistent within statistical error to the data with the spikes removed.

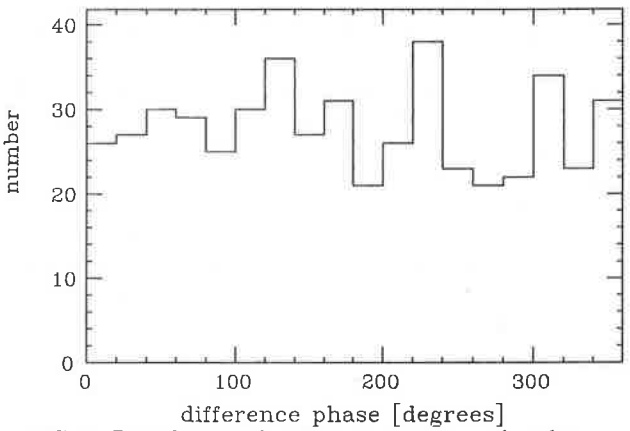

FIG. 7. Distribution of positive or negative spikes that were removed in the data analysis before the fit as a function of the difference phase, ϕ_d. No correlation at $2\phi_d$ could be found.

The temperature and pressure measurements were averaged over the length of a cut. These mean values were used to apply corrections as described below and in section III C.

xxx second data analysis 2ppm....

VI. ATTRACTOR MASS METROLOGY

Our largest systematic uncertainty was due to the attractor mass distance measurement from which the dominant attracting moment Q_{22} was calculated. The position of the spheres were measured before and after each data run. We measured the horizontal distance of the upper two spheres and the vertical distance between spheres on each side of the pendulum. Specially fabricated micrometer tools made primarily of Invar were used for the horizontal distance measurement between the outer faces of the spheres. Immediately before and after each distance measurement the tool was compared to a specially made Invar ball bar standard. The vertical spacing between the spheres was measured by inserting a small gauge block that was ≈10-20 μm thinner than the height of the gap between the sphere surfaces. We inferred the spacing by measuring the small angle by which the gauge block could be tilted before it touched the surface of both spheres. This tilt angle was measured with a laser beam that was reflected off a mirror attached to the gauge block. The diameters of the spheres were measured in the same places on the spheres as used for the distance measurements between the spheres. The temperature of the attractor mass was recorded during the distance measurements.

The Invar ball bar standards that we used were made to within about $\pm 15\mu$m of the lengths that had to be measured. The bars were calibrated at NIST to within 0.4 μm (k=2, 2σ) [20]. The C-shaped micrometers had a polished tungsten carbide steel stop on one end and a precision dial indicator on the other end. The short, ≈100μm, total range of the dial indicators was checked for overall linearity and calibration using a separate precision screw micrometer. In addition the dial indicators were occasionally moved by small amounts relative to the other stop of the micrometer, so that several different regions in dial indicator's travel were used.

The temperature of the attractor turntable was continously measured. The data were used to provide a continuous correction to account for the thermal expansion of the attractor mass assembly. Since the turntable was made from the same Aluminum one expansion coefficient could be used, which was 23×10^{-6} K^{-1}. While distance measurements on the attractor mass arrangement were performed, the temperature of the turntable was measured. During the measurement the attractor temperatures drifted by about ± 0.1 K. As the temperature distribution within the attractor could not be determined exactly we assigned a 0.1 K temperature uncertainty to the distance measurements. A small temperature correction was applied to the ball bar length to reference it to the temperature at which it was calibrated at NIST (<0.5 μm).

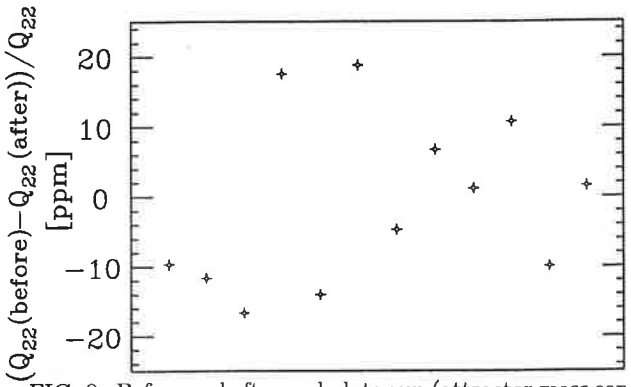

FIG. 8. Before and after each data run (attractor mass configuration) the coordinates of the spheres were measured. The plot shows the fractional difference in Q_{22} determined before each run and after each run. The average of Q_{22}(before) and Q_{22}(after) of each configuration was used in the data analysis.

The overall precision of our G-measurement could be improved by a more precise, continuous distance measurement scheme, perhaps by using an interferometric scheme or by using a coordinate measuring machine (as was done in ref [21]).

VII. UNCERTAINTIES, SYSTEMATIC EFFECTS AND TESTS

In Table I we list the time-constant corrections that were applied to the data. The DSP was programmed to average all data over $\tau = 1$ s intervals. The true amplitudes of the sinusoidal signal at frequency $2\omega_d$ were attenuated by a small amount: $\frac{\sin(\omega_d \tau)}{\omega_d \tau}$. More importantly the two successive numerical derivatives of $\sin(2\omega_d t)$ were smaller than the analytic derivatives by $(\frac{\sin(\omega_d \Delta t)}{\omega_d \Delta t})^2$, where Δt was the chosen time increment. For the attenuation coefficients to became simple and exact it was important that ω_d could be held constant. Since these corrections were substantial we analyzed the data using a wide variety of different increments and found that our results were independent of the choice of Δt within statistical uncertainties. We chose an increment of $\Delta t = 10$ s as a compromise between the noise amplitude in α and size of the correction.

TABLE I. Summary of constant correction factors.

finite pendulum thickness	1.0007857
pendulum attachment and imperfections	1.0000433
swing damper twist	1.0000060
α_{62}-correction	0.9998767
α_{82}-correction	0.9999951
data averaging ($\tau = 1$ s, $\omega_d = 20$ mrad/s)	1.0000667
numeric derivatives ($\Delta t = 10$ s, $\omega_d = 20$ mrad/s)	1.0134544
Total:	1.0142322

We tested the accuracy of the entire data analysis with numerically simulated data . We used an equation of motion for the pendulum that included the gravitational signal of interest, the gravitational room background, fiber drift, DC torques and torque noise. For the latter we assumed $1/f$-noise that was mimicked by "random walk with turn-around". The equation of motion was integrated twice and then white angle-read-noise was added. Fig. 9 shows the typical residuals of a fit to the simulation compared to the residuals from real data. The noise of the simulation closely emulates the noise in the data. Our data-analysis software accurately reproduced the value of G that we assumed in the equation of motion, which verified the attenuation factors. We tested various values of G, strongly exaggerated room background, drift, DC torques, noise etc., and found no dependence within statistical uncertainty.

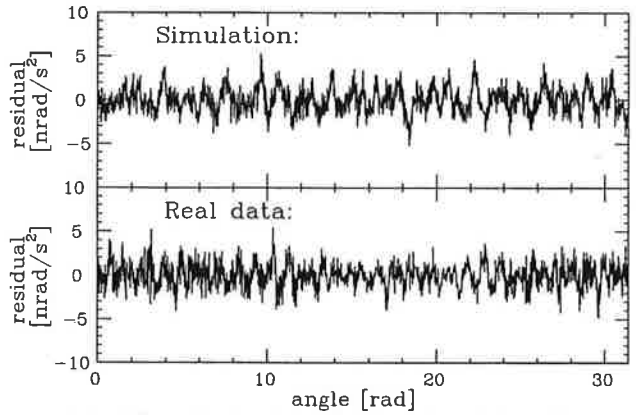

FIG. 9. Fit residuals of simulated and real data. Note the similarity of the noise of the simulations to the observed noise. The simulations were used to verify the accuracy of the data reduction.

Numeric modeling of pendulum-attractor interaction not using the multipole formalism was performed to test the accuracy (and correctness) of the corrections of Eqs. 1, 9,10. These models were also used to determine the sensitivity to pendulum imperfections and misalignments. Because of the symmetry of the pendulum and attractor mass configuration effects due to misalignments behave quadratically in displacement. They were found to be negligible. For example, a 0.1 mm horizontal attractor mass misalignment would change the signal by only $\approx$1 ppm.

The analysis on the entire data set was carried out by two people in parallel without knowing each others results. The final results differed by only 2 ppm. On a small subset of the data we tested an independent (and less automated data analysis) using different software. The results were identical.

The pendulum was surveyed using a measuring microscope. The difficulty in accurately assessing the pendulum flatness with the measuring microscope is reflected in the considerable uncertainty of 4μm.

The lab-fixed horizontal magnetic field at the apparatus was measured to be $\approx$100 mG. We ran tests by exaggerating the stationary field at the location of the μ-metal shield in which the pendulum was housed to $\approx$5 G and at the location of the spheres to $\approx$100 G. The observed acceleration difference due to the exaggerated fields was $(6\pm8)\times10^{-12}$ rad/s^2. In another magnetic test a small permanent magnet was installed on the attractor turntable in a position similar to that of the spheres. The field this magnet would have caused at the location of the pendulum if no μ-metal shield had been present was $\approx$0.330 G. A small brass weight was installed on the turntable at an angle 90° azimuthally from the permanent magnet to compensate the gravitational coupling of the magnet. In a short run the acceleration was measured to be $\ll 7\times10^{-11}$ rad/s^2. The magnetic field fixed to the stainless steel attractor spheres was measured to be $\ll$0.5 mG at about 2.5 cm from the sphere surfaces. From all the magnetic tests an upper limit on magnetic accelerations of 0.6 ppm was established.

To investigate the rotating temperature gradient sensitivity, two 5 W resistive heaters were installed in the place of spheres on the rotating attractor turntable. These heaters exaggerated the normally observed temperature variation at $2\omega_d$ by a factor of more than 250, as measured by the air temperature sensor attached to the rotating vacuum can in the space between the vacuum can and the spheres. This sensor was placed to be most sensitive to a potential temperature gradient due to the spheres. The acceleration amplitude with the heaters

TABLE II. One σ error budget.

quantity	measurement uncertainty	$\Delta G/G$ (ppm)
Systematic errors:		
pendulum:		
width	< 20 μm	0.4
thickness & flatness	< 4.0 μm	4.0
attractor masses:		
diagonal separation	< 1.0 μm	6.9
ball-bar calibration	< 0.2 μm	1.4
vertical separation	< 1.0 μm	5.3
sphere diameter	< 1.5 μm	2.4
temperature uncertainty	< 100 mK	6.9
mass	< 3.0 mg	0.4
air humidity		0.5
residual twist angle:		0.3
magnetic fields:		0.6
rot. temperature grad.:		0.4
time base:	$< 10^{-7}$	0.1
data reduction:		2.0
Statistical error:		5.8
Total:		13.7

activated vs. not differed by $|\Delta\alpha| = (21 \pm 22) \times 10^{-12}$ rad/s^2. Therefore the rotating temperature gradient coupled signal during G-measurements was $< 2 \times 10^{-13}$ rad/s^2 (0.4 ppm). This temperature uncertainty is not to be confused with the attractor mass temperature uncertainty leading to thermal expansion i.e. Q_{22} uncertainty (section VI).

The overall linearity and insensitivity to the signals at $4\omega_d$ was tested using two pairs of spheres separated by 45° of azimuth on each side. This 8-sphere configuration was assembled from two normal 4-sphere configurations. One of the 4-sphere configurations was measured before the 8-sphere configuration and the other 4-sphere configuration was measured after the 8-sphere configuration was measured. The 8-sphere measurement was 12.7±9.6 ppm (stat. error only) higher than the combined 4-sphere results. Since the two configuration types agree well enough and our method (as well as gravity) is linear the result of this test was not added into the error budget.

The turntable itself, without the attractor spheres on it, produced a small $\sin(2\omega_d t)$ gravitational acceleration signal of amplitude $\approx 8 \times 10^{-11}$ rad/s^2. This contribution was automatically subtracted out by combining different attractor mass configuration pairs. Changes in attractor turntable Q_{22} due to load changes within configuration pairs were estimated to be negligible.

Due to the large but finite gain ($>3\times10^6$) of the acceleration feedback loop a very small twist remained in the fiber. The twist angle component at $2\omega_d$ was phase shifted and poorly resolved so that an upper limit of ±0.35 ppm error was used instead of a correction.

The systematic uncertainties that were most difficult to quantify were those associated with the length measurements on the attractor masses. A 1μm measurement uncertainty was used to include potential problems that may have arisen since the ends of the ball bars that were used to calibrate the micrometers and our attractor spheres had different radii of curvature. The actual readability and reproducibility of the length readings was better than 1μm. We measured the vertical distance between the spheres using a micrometer as well as the gauge block tilt method (described in sec. VI). These two methods gave consistent results after a small (1μm) length change due to the vertical micrometer's own weight was included. The micrometer had initially been calibrated held in a horizontal position. The instrument constructed to measure the diameter of the spheres was more difficult to calibrate and therefore a more generous systematic uncertainty was assumed. The effect of the sphere diameter uncertainty on the Q_{22} determination was weakened since the sphere diameter was subtracted from the horizontal distance measurement to give the distance between the spheres centers of mass while the sphere diameter was added to infer the vertical center of mass separation. The sensitivity of the two measurements to the sphere diameter cancels to ≈77%.

Using spheres as attractor masses was advantageous as the masses could be placed in specific orientations to systematically reduce the sensitivity to density inhomogeneities (section IV B). Additionally the density uncertainties were diminished by the use of four spheres in each configuration and two independent sets of spheres. Compared to other experiments the distance from the pendulum to the attractor masses was relatively large, which weakened the effect of density fluctuations from the outset. We made several estimates of density fluctuation uncertainties, which all led to negligible effects. The sensitivity to surface undulations was small for the same reasons. Nevertheless the sphere diameter measurements were included in the calculation of the Q_{22}s.

The Statistical uncertainty for each configuration was derived from the variance of the fit results of >50 data cuts. To combine the six configurations we adopted the worst statistical uncertainty of the six configurations for all the configurations.

VIII. RESULTS AND DISCUSSION

We combined the results from the different attractor mass configurations into pairs that eliminated accelerations due to the attractor turntable itself. The average of three pairs yielded our G-value (Fig. 10).

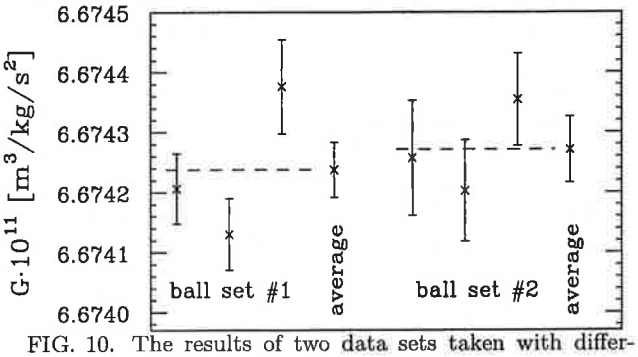

FIG. 10. The results of two data sets taken with different spheres. Each data point is the combination of a pair of attractor configurations. Within each pair accelerations due to interactions the attractor turntable itself are eliminated. Combining the three pairs taken with different sphere orientations optimally reduced effects from sphere-density and shape imperfections. The displayed uncertainties are statistical only.

Combining the two G-values obtained with different spheres resulted in our gravitational constant to be:

$$G = (6.674255 \pm 0.000092) \times 10^{-11} \text{ m}^3 \text{ kg}^{-1} \text{ s}^{-2}. \quad (11)$$

The systematic and statistical uncertainties are shown in Table II. The total uncertainty is the quadrature sum of the individual uncertainties.

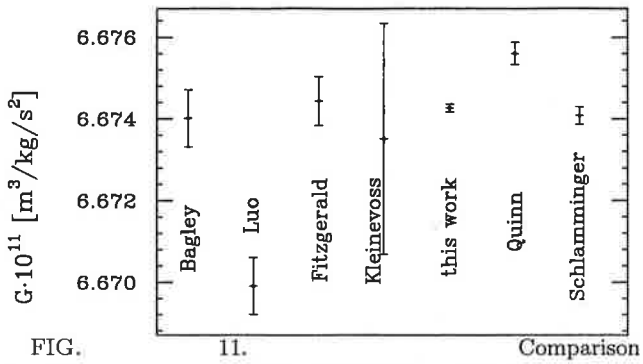

FIG. 11. Comparison to other measurements [7,3,4,6,14,21,22] published after 1995 and with $\Delta G/G < 1000$ ppm.

Our measurement indicates a value of G that is about 2σ larger than the 1986 accepted value, but fits well within the large uncertainty limits of the 1998 accepted value. Fig. 11 compares our results to other recent measurements. The values labeled Bagley, Luo, Fitzgerald and Quinn were also obtained with torsion balances, all operated in different modes. Kleinevoss' value was obtained with a pair of vertical pendulums and Schlamminger's value with a beam balance. We regard the measurements with substantially different approaches as particularly valuable as they may not be subject to the same undiscovered systematic errors. Two high precision measurements were published after the first publication of our measurement: Quinn et al. [21] used a strip torsion balance and obtained data in two different operating modes: electrostatic feedback and calibrated deflection. Their value is 4.5 of the combined standard deviations higher than our value. Schlamminger at al. [22] used the Poynting method employing a modern beam balance and two large tanks of Hg. Their value is 28 ppm lower than ours, but in good agreement within uncertainties.

The method that we used for this measurement of G has several advantages over traditional torsion balance setups:
-Highly reduced uncertainty from the pendulum mass distribution
-Torsion fiber properties do not affect the measurement (Kuroda bias)
-High signal frequency leads to reduced statistical noise

In comparison to other measurements of G we were able to substantially reduce the systematic as well as the statistical uncertainties. Apart from the lengths calibrations for the attractor mass configuration no cumbersome calibrations had to be carried out. Since the largest limitation in our measurement is due to the attractor mass metrology our overall precision could be improved by for instance with an interferometer scheme to measure the relevant distances more accurately. Improvement in the temperature control of the attractor mass assembly would be desired. A set of denser attractor masses, which could for example be made from tungsten, would double the signal strength. Similar-sized tungsten spheres with very high tolerances have been machined for the measurement by Luther [8]. A more massive pendulum plate, which could be manufactured from molybdenum, would likely reduce the statistical noise.

Our method presents a new operation mode of a torsion balance that may also have other useful applications in measuring small forces or torques quantitatively. Several aspects of our technique may be applicable to other torsion balance measurements techniques of G: for instance the use of a plate pendulum would lead to similar advantages using the time-of-swing method.

Combining our value of G with the geocentric value $GM_\oplus = (3.986004418 \pm 0.000000008) \times 10^{14}$ m^3 s^{-2} [23] obtained from precise laser ranging to the LAGEOS satellite we determine the total mass of the Earth to be

$$M_\oplus = (5.972209 \pm 0.000082) \times 10^{24} \text{ kg}. \quad (12)$$

Likewise, using $GM_\odot$ [24], the mass of the Sun is

$$M_\odot = (1.988423 \pm 0.000027) \times 10^{30} \text{ kg}. \quad (13)$$

IX. ACKNOWLEDGEMENTS

We wish to thank the members of the Eöt-Wash group and Maximilian Schlosshauer for writing the data simulations. We thank the National Institute of Standards and Technology for the support of this work with precision measurement grant # 60NANB7D0053 and for calibrating our length standards [20]. This work received additional support from the National Science Foundation through grant # PHY-9602494 to the Eöt-Wash group. Further assistance was provided by the Physics Department of the University of Washington through machine shop time, and with technical services and infrastructure from the Nuclear Physics Laboratory (now CENPA), which is supported by the Department of Energy.

[1] V.P. Izmailov, et al., Measurement Techniques **36**, 1065 (1993).
[2] W. Michaelis, H. Haars, and R. Augustin, Metrologia **32**, 267 (1995).
[3] J. Luo, et al., Phys. Rev. D **59**, 042001 (1998).
[4] M.P. Fitzgerald and T.R. Armstrong, Meas. Sci. Technol. **10**, 439, (1999).
[5] F. Nolting, J. Schurr, S. Schlamminger, and W. Kündig, Meas. Sci. Technol. **10**, 487, (1999).
[6] U. Kleinevoss, H. Meyer, A. Schumacher, and S. Hartmann, Meas. Sci. Technol. **10**, 492, (1999).
[7] C.H. Bagley and G.G. Luther, Phys. Rev. Lett. **78**, 3047 (1997).
[8] G.G. Luther and W.R. Towler, Phys. Rev. Lett., **48**, 121 (1982).

[9] E.R. Cohen and B.N. Taylor, Rev. Mod. Phys., **59** 1121 (1987).
[10] P.J. Mohr and B.N. Taylor, J. Phys. Chem. Ref. Data, **28** 1713 (1999).
[11] Kazuaki Kuroda, Phys. Rev. Lett. **75**, 2796 (1995).
[12] S. Matsumura, et al., Phys. Lett. **A244**, 4 (1998).
[13] J.H. Gundlach, E.G. Adelberger, B.R. Heckel and H.E. Swanson, Phys. Rev. D **54**, R1256 (1996).
[14] J.H. Gundlach and S.M. Merkowitz, Phys. Rev. Lett. **85**, 2869 (2000).
[15] R.D. Rose et al., Phys. Rev. Lett. **23**, 655 (1969).
[16] Y. Su, et al., Phys. Rev. D **50**, 3614 (1994).
[17] The experiment is located at 47.66°N, 122.30°W about 29 m above sealevel.
[18] Weighed at Quality Control Services, Inc., Portland Oregon. Traceable certificate #1170W.
[19] CRC Handbook of Chemistry and Physics, 65^{th} Edition, p. F-8,9.
[20] D. Everett and J. Stone, NIST Engineering Metrology Group, Test report, internal control #M6482.
[21] T.J. Quinn et al., Phys. Rev. Lett. **87**, 111101-1 (2001).
[22] St. Schlamminger, E. Holzschuh, W. Kündig, Phys. Rev. Lett. **89**, 161102-1 (2002).
[23] J.C. Ries, R.J. Eanes, C.K. Shum, M.M. Watkins, Geophys. Res. Lett. **19**, 529 (1992).
[24] Astronomical Almanac for 2001, US Government Publishing Office, p. k6 (1999).